Development of Porous UHMWPE Morphologies for Fixation of Gel-Based Materials

Kevin Plumlee, Christian J. Schwartz

Department of Mechanical Engineering, Texas A & M University, College Station, Texas 77843

Received 2 February 2009; accepted 22 May 2009
DOI 10.1002/app.30801
Published online 7 July 2009 in Wiley InterScience (www.interscience.wiley.com).

ABSTRACT: Novel gel-based materials including hydrogels and bioderived polymers show great potential in orthopedics but require a means of mechanical fixation to a substrate. The development of controlled porous ultra-high-molecular-weight polyethylene (UHMWPE) morphologies is targeted to expand the future potential for UHMWPE-based composites with such novel bioderived materials. Porous UHMWPE morphologies were produced by means of a sodium chloride leaching process. Compression-molded samples were prepared by dry mixing of sized NaCl particles and UHMWPE powder. These were then soaked in water to remove the porogen, leaving a porous UHMWPE structure. The mass of removed porogen and resulting void density were found to match well with Monte Carlo simulations. Distribution of NaCl particles was greatly influenced by the ratio of particle sizes between NaCl and UHMWPE. Limited percolation was achievable at NaCl concentrations below 50 wt %, whereas porogen concentrations above 60 wt % led to interconnected networks. Porous UHMWPE scaffolds were impregnated with gelatin to explore the penetration of a gel-based phase. It was observed that the gelatin was able to permeate the UHMWPE to a great extent, except for unfilled voids due either to entrapped air or insufficient channel diameters to accommodate gelatin flow. These results confirm that porous morphologies can be created in a controlled manner and tailored for chosen applications. © 2009 Wiley Periodicals, Inc. J Appl Polym Sci 114: 2555–2563, 2009

Key words: polyethylene (PE); biomaterials; mixing; interpenetrating networks (IPN); implant

INTRODUCTION

Ultra-high-molecular-weight polyethylene (UHMWPE) remains the most widely used material for bearing surfaces in artificial joint applications involving articulation against a metallic counterface. Despite its high durability, low coefficient of friction, and biocompatibility in bulk form, studies have revealed that wear particulate shed from UHMWPE is responsible for initiating osteolysis, a degeneration of the bone surrounding the implant, ultimately limiting the lifespan of the device.[1]

A significant amount of research has centered on reducing osteolysis by decreasing the production rate of wear particulate. Crosslinking has been shown to significantly reduce the wear rate of UHMWPE,[2–5] but it also decreases elongation at break and impact toughness.[6–9] In attempts to mitigate property deficiencies associated with crosslinking, some researchers have investigated composites. Tanniru and Misra[10] found that the inclusion of inorganic calcium carbonate particles increased the impact toughness of UHMWPE by up to 50% to counteract the detriment caused by crosslinking. Guofang et al.[11] incorporated the mineral kaolin during UHMWPE polymerization and reduced the wear rate by over 40%, enough to be nearly comparable to crosslinking. Similar results were found using quartz,[12] alumina,[13] quasicrystals,[14] carbon fiber,[15] and a variety of nanofillers such as carbon nanotubes.[16] The use of more compliant materials, both as a stand-alone bearing material[17] and as a composite constituent,[18,19] may reduce contact pressures and friction coefficients at wear interfaces, thereby reducing the total wear rate. However, the biocompatibility of many of these materials is not well established, and thus, other avenues must continue to be investigated.

As opposed to simply decreasing the wear volume, another possible approach revolves around making the wear debris exhibit less potential for osteolysis. Researchers have explored this avenue by filling UHMWPE with materials naturally found in the human body, including hyaluronan[20] and hydroxyapatite.[21] In general, these types of fillers have provided similar wear reduction as seen with inorganic composite fillers, but they still fail to mimic the advantageous properties of natural cartilage found in healthy joints. Studies have shown that osteolysis is triggered predominately by wear particles between 0.1 and 1 μm in diameter,[22,23] and most *in vivo* wear particulate falls within this range.[24,25] Therefore, modifying the material such

Correspondence to: C. J. Schwartz (cschwartz@tamu.edu).

that the wear debris is drastically larger or smaller may reduce the osteolytic effect.

Much biomedical research has recently revolved around materials that more closely approximate living tissue. In particular, hydrogels have found numerous applications as scaffolds, drug delivery media, and as cell growth stimulants.[26] A hydrogel's capacity to mimic aspects of the extracellular matrix of living soft tissues makes them prime candidates for use as synthetic cartilage in orthopedic-bearing applications. Although these materials provide excellent shock absorption and lubricant transfer when compared with UHMWPE, their poor mechanical properties and resulting poor wear performance limit their immediate value in artificial joints. Oka et al. and Suciu et al. both report hydrogel wear rates at least an order of magnitude greater than rates typically seen in noncrosslinked UHMWPE,[27,28] whereas interactions between the hydrated hydrogel and natural lubricants create a complex tribological process that makes long-term behavior difficult to predict.[29] Work has been done to produce gel-like materials from synovial components, such as chondroitin sulfate,[30] hyaluronic acid,[31] and polysaccharides.[32] The development of these materials may provide groundwork for bioderived-bearing surface materials that do not induce the osteolytic response.

Although not as predominant as hydrogels in the field of tissue engineering, porous UHMWPE porous scaffolding has been investigated for nonload- bearing medical applications because of its durability, chemical inertness, and biocompatibility. Frequently used in facial reconstruction surgeries[33] and filtration membranes,[34] such components are often created through a porogen leaching process in which the samples are initially created with an dissolvable porogen, such as salt, dispersed throughout the sample. The sample is then soaked in a solvent that dissolves away the porogen, leaving voids within the polymer. Leaching techniques are cost-effective solutions for producing a wide range of polymeric porous structures.[35–38] Even when held at a constant porosity, controlling the size and shape of the porogen also can result in variable mechanical properties.[39,40]

Typical studies into porous UHMWPE leave the pores vacant, allowing for cell ingrowth or fluid flow through the sample. However, filling the pores of porous UHMWPE with a complimentary material, such as a hydrogel, may result in distinct advantages for artificial joint applications. One possibility may involve the hydrogel phase infused with therapeutic compounds such that as the bearing surface wears, the compound is released into the joint, counteracting the osteolytic effect of the wear particulate. Producing an ideal balance of wear resistance, shock absorption, and lubrication for a particular application might then be attained by tailoring the ratio of hydrogel to UHMWPE. Ultimately, the reduction or elimination of osteolysis may allow for longer lifetimes of implanted devices.

The goal of this work was to combine the advantages of both UHMWPE and hydrogels by determining the feasibility of producing a composite of the two. First, the creation of tailored porous UHMWPE through porogen leaching was examined through mathematical models and parallel physical experiments. Porous samples were then impregnated with gelatin to observe the interaction and penetration of a hydrogel in a hydrophobic scaffold.

MATERIALS AND METHODS

Numerical modeling

To create a porous UHMWPE scaffold through salt leaching, a UHMWPE matrix with well-dispersed salt granules is a necessary first step. To achieve this, medical-grade UHMWPE powder (GUR 1050, Ticona) was dry mixed with NaCl crystals, then compressed under heat and pressure into a solid block. It has been suggested by previous studies that the ratio of matrix particle size to filler particle size greatly influenced the final distribution of filler particles within the fully formed composite. In an effort to understand the relationship between the porogen (NaCl) and polymer particles during the dry powder mixing process, Monte Carlo simulation models were created in MATLAB® to represent the distribution of particles within a sample volume, and the maximum possible void volume resulting from an initial amount of porogen in the UHMWPE.

The basic strategy of the powder dispersion model was to create a visual representation of a two-dimensional slice of the final UHMWPE–NaCl composite based on the volume percent and initial particle size of the two constituents. An empty 2D array represented a sample area, and representations of individual particles populated an array representing the material type (matrix or porogen) in all of the individual locations in the array. A virtual particle, either porogen or matrix type, was randomly placed along the top of the array, and then lowered through the empty space until another particle was encountered. This position in the array was then filled, and another particle began the process. This was repeated until the array was filled. The graphic results of the simulation allowed for visual comparison of the particle distribution associated with various particle sizes.

A second simulation was developed to demonstrate the behavior during the process of a solution (water) dissolving the porogen (NaCl) particles over time within the UHMWPE matrix, known as the

leaching process. A three-dimensional array representative of a sample volume was filled with the appropriate number and size of randomly placed porogen particles. This array was then subjected to a virtual leaching process by removing porogen particles that were exposed to an outside surface or empty region. As particles were removed, new empty regions were created within the matrix. Starting at the outside edges and working inward, the simulated dissolution process repeated until no further porogen particles could be removed. The final porosity and remaining volume percent of porogen were then calculated. This allowed for comparisons of multiple samples with varied porogen concentrations and particle sizes.

Sample fabrication

Sodium chloride (OmniPur, EMD) was chosen as a porogen because of its availability, solubility in water, and biocompatibility. To control the particle size, NaCl was ground with a mortar and pestle, then sieved into two separate batches: one consisting of particles less than 100 μm and the other of particles between 100 and 300 μm. The two different batches will be referred to as small and large particles, respectively. Granulated UHMWPE with an average particle size of $\sim$ 140 μm was added to the particles to create multiple powder mixtures ranging from 10 to 85% porogen, by weight, all of which were mixed in a vortex mixer. These mixtures were then compression molded at 230°C and 100 MPa for 10 min to create cylindrical samples of 6.54 mm in diameter and $\sim$ 15 mm long.

After formation, the sample weights were recorded. The samples were placed in a beaker of deionized water in an ultrasonic bath for a total of 5 h to leach out the imbedded porogen. The water was replaced every 30 min during the first 2 h of soaking, then periodically throughout the rest of the soak cycle. At the completion of the leaching process, all the samples were thoroughly dried and weighed. The weight loss of each sample was compared to the predictions made by the three-dimensional numerical model.

After leaching, selected samples were imaged in a JOEL-6400 scanning electron microscope. Samples were prepared for imaging first with a ruthenium vapor coating technique,[41] then with a light sputter coating of gold–palladium. The ruthenium vapor coating was chosen to prove a more even coating on the highly porous surfaces than sputter coating alone.

Gel-phase impregnation and imaging

To investigate the viability of using porous UHMWPE as a fixation scaffolding for various soft tissues and gels, leached and dried samples were impregnated with gelatin and then imaged in the SEM. A procedure for preparing samples was developed specifically for SEM imaging and is described later. This chemical treatment process allows the gelatin to retain its structure while under the high vacuum of the SEM and improves the contrast between the UHMWPE scaffolds and the gelatin when viewed with backscattered electron detection through the addition of gold nanoparticles to the gelatin phase. This procedure would not be necessary for generic preparation of mechanical samples.

A total of 0.35 g of gelatin (Knox) was mixed with colloidal gold (25 nm diameter, Anderson Laboratories) in 10 mL of distilled water. This mixture was heated to a boil, then the cylindrical porous UHMWPE samples were submerged into the resulting liquid. The entire setup was placed under intermittent vacuum of 380 mmHg to increase the penetration of the gelatin into the pores of the UHMWPE. After 15 min under vacuum, the mixture was chilled in a refrigerator for 2–3 h to allow the gelatin to solidify, after which, the impregnated UHMWPE samples were removed. These samples were immediately placed into a 10% (vol/vol) aqueous acrolein (Electron Microscopy Sciences) solution to crosslink the gelatin, preventing the structure from degrading during the drying process. After crosslinking, samples were rinsed in three changes of deionized water and then dehydrated in successive concentrations of methyl alcohol in water, ranging from 10 to 100% alcohol. Finally, thin slices from the centermost region of the samples were removed using a fresh razor blade. These sections were then submerged in three changes of hexamethyldisilazane (HMDS, Electron Microscopy Sciences), a chemical critical point drying solution, then carbon coated for SEM imaging.

RESULTS AND DISCUSSION

Modeling results

The powder dispersion model described earlier produced a visual representation of cross-sections of a virtual sample. Representations of particle distributions for a variety of initial particles sizes were produced using the powder dispersion model. For every run, both the volume percent and porogen particle size were held constant while the initial size of the matrix particles was increased. These results, shown in Figure 1, reveal distinct differences in the dispersion quality as the ratio of matrix-to-porogen particle sizes increased. As expected, the particle size ratio of 1 : 1 (matrix/porogen) generates a mixture that is most uniform. As the ratio is modified in either direction from unity, the dispersion quality

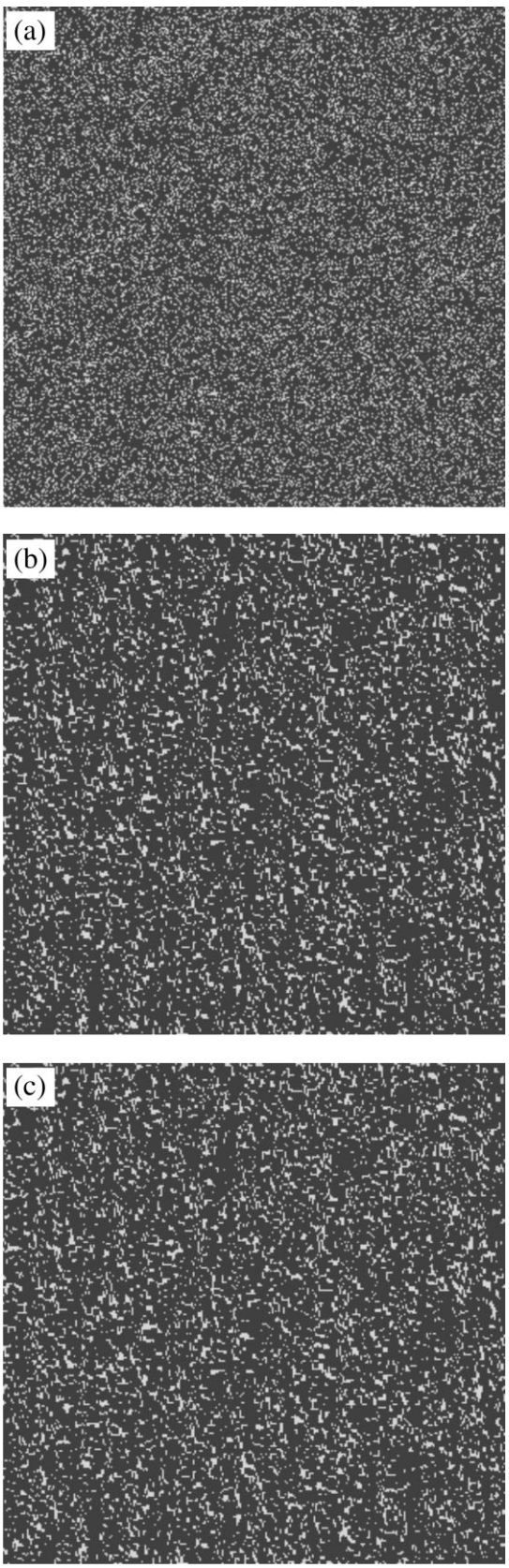

Figure 1 Monte Carlo simulation results of sample distributions of porogen (light) and matrix particles (dark) during dry powder mixing. Porogen particles make up 20% of the total area of each image. The ratio of matrix particle size to porogen particle size is (a) 1 : 1, (b) 4 : 1, and (c) 1 : 4.

decreases. When the UHMWPE particles are significantly greater than the NaCl particles, the matrix tends to clump together and have large areas without porosity. Compare this result to the situation when the porogen particles are significantly larger than the matrix particles. In the latter scenario, distribution is still poor but the porogen particles tend to agglomerate into large volumes at the borders of the matrix particles. This suggests that the resulting porous polymer may have less integrity at a chosen fill percentage than if the matrix particles were larger than the porogen.

In many composite applications, the ideal mixture is uniform, indicating that the ideal particle size ratio is 1 : 1. In the cases of greatly different ratios, the porogen particles must migrate away from each other through the melted matrix during the molding process for the final product to become uniform. This would require that the porogen particles have no mutual attraction, and that the duration of elevated temperature allows for complete diffusion. In this study, the high melt viscosity of UHMWPE prevented this particle motion, and therefore, the simulations did not account for particle agglomeration.

Although many composite applications seek uniform particle distributions, the leaching process does not necessitate such uniformity. It requires only that the NaCl particles achieve percolation (removal of porogen from the UHMWPE matrix) to allow for full leaching, and that the matrix remains interconnected so that the resulting porous structure remains in one piece. In this regard, using a size ratio greater than 1 : 1 may prove beneficial by forcing the NaCl particles to accumulate in interconnected veins that run through the entirety of the sample, allowing for percolation of at lower fill contents. Using this technique may also result in many of the final pores being much greater in size than the individual porogen particle size because of the accumulation of particles, even at low fill contents. To explore these phenomena, physical samples were made with two different sizes of porogen particles: one batch approximately equal to the matrix particle size, whereas the other batch contained particles much smaller than the matrix particles.

Percolation results

The three-dimensional percolation Monte Carlo simulation predicted the total volume of porogen that could be released dependent on sample geometry, pore size, and fill content. The simulation calculates the porosity of the sample after the leaching process, that is, the percentage of the original sample volume that becomes void after leaching. One area of interest was whether there would be a difference between samples of the same fill content but different porogen

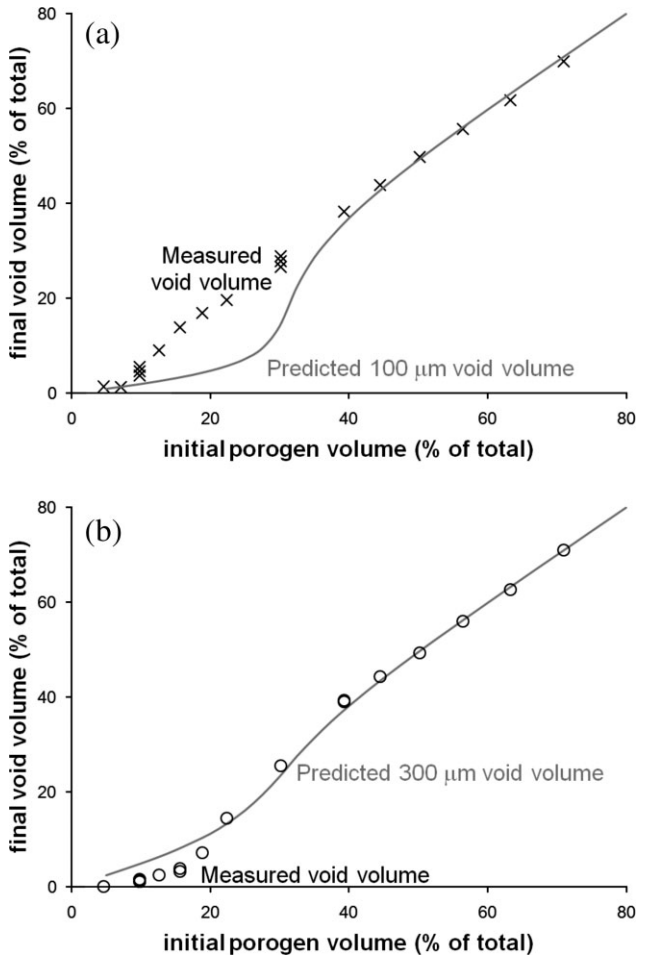

Figure 2 Comparison of the simulation and actual results of porogen leaching. Simulated porogen particle sizes used were as follows: (a) 100 μm and (b) 300 μm.

particle sizes. For the samples created with smaller porogen particles, the powder dispersion model predicts the accumulation of vein-like bands of particles throughout the sample. It was expected that these structures would improve percolation, especially at lower fill contents. Figure 2 illustrates the resulting void volume after leaching the porogen-filled UHMWPE samples along with the model predictions for samples produced with small NaCl particles (<100 μm) and large NaCl particles (100–300 μm).

The aspect of these results that is most apparent is that there is relatively good agreement with the simulation for the larger porogen size, showing that there is a knee in the leaching behavior that occurs between ~ 20 and 40% initial porogen volume. At higher fill volumes, it is apparent both from the simulation and the test results that nearly all of the porogen are removed during leaching. The presence of the knee in the data indicates the fact that the large particles have a higher probability of contact with each other at lower fill percentages than do smaller particles. It is estimated from the results that the porogen particles begin to achieve interconnectedness at around 20 vol % fill. In contrast, the small porogen particle results do not agree well with the simulation below 40%. The simulation underestimates the amount of NaCl removed at these fill proportions. The experimental data do not show a clearly visible knee to suggest an abrupt onset of interconnectedness of voids, but rather appear to follow a linear trend over all fill percents. This may be due to the fact that the smaller particles are more apt to produce a vein-like structure within the UHMWPE that allows for more complete leaching than with the larger porogen particles. As with the large particles, the experimental data and simulation agree well at higher fill percents. As previously mentioned, the simulation model assumes a random dispersion of porogen particles, implying that each particle has a specific likelihood that it will connect with another particle. This probability is dependent on the volume percent of porogen within the sample, but not the particle size. When considering interconnected networks, the propagation of probability requires that longer chains of multiple particles are less likely than chains of fewer particles.

To examine the internal porous structure of the leached UHMWPE samples, they were sliced in half with a razor blade, and the exposed surfaces were imaged in the SEM. These images are shown in Figure 3. UHMWPE samples with larger NaCl particle sizes revealed a well-defined porous structure defined by individual cubic NaCl crystals. Pores were interconnected through the overlapping of large single crystal formations, and the interior walls of the pores appeared relatively smooth. In contrast, the samples made with smaller NaCl particles revealed a less orderly porous structure. Within these samples, the larger regions of pores were not uniform in size or geometry and were interconnected through thin branching of smaller pores. Interior surfaces were noticeably rougher than in samples made from large particles. This type of structure is consistent with the marbled appearance and particle accumulation predicted by the two-dimensional mixing model. These results support the claim that the average pore size, geometry, and porosity can be tailored through the control of the porogen and matrix particle size and quantity.

Impregnation results

The porous UHMWPE samples impregnated with gelatin were imaged with the SEM using both secondary and backscatter mode to reveal the structure of the composite. The secondary images revealed the overall distribution and geometry of pores, but offered very little information regarding behavior of the gelatin. As seen in Figure 4, the backscattered images clearly showed the location of gelatin within

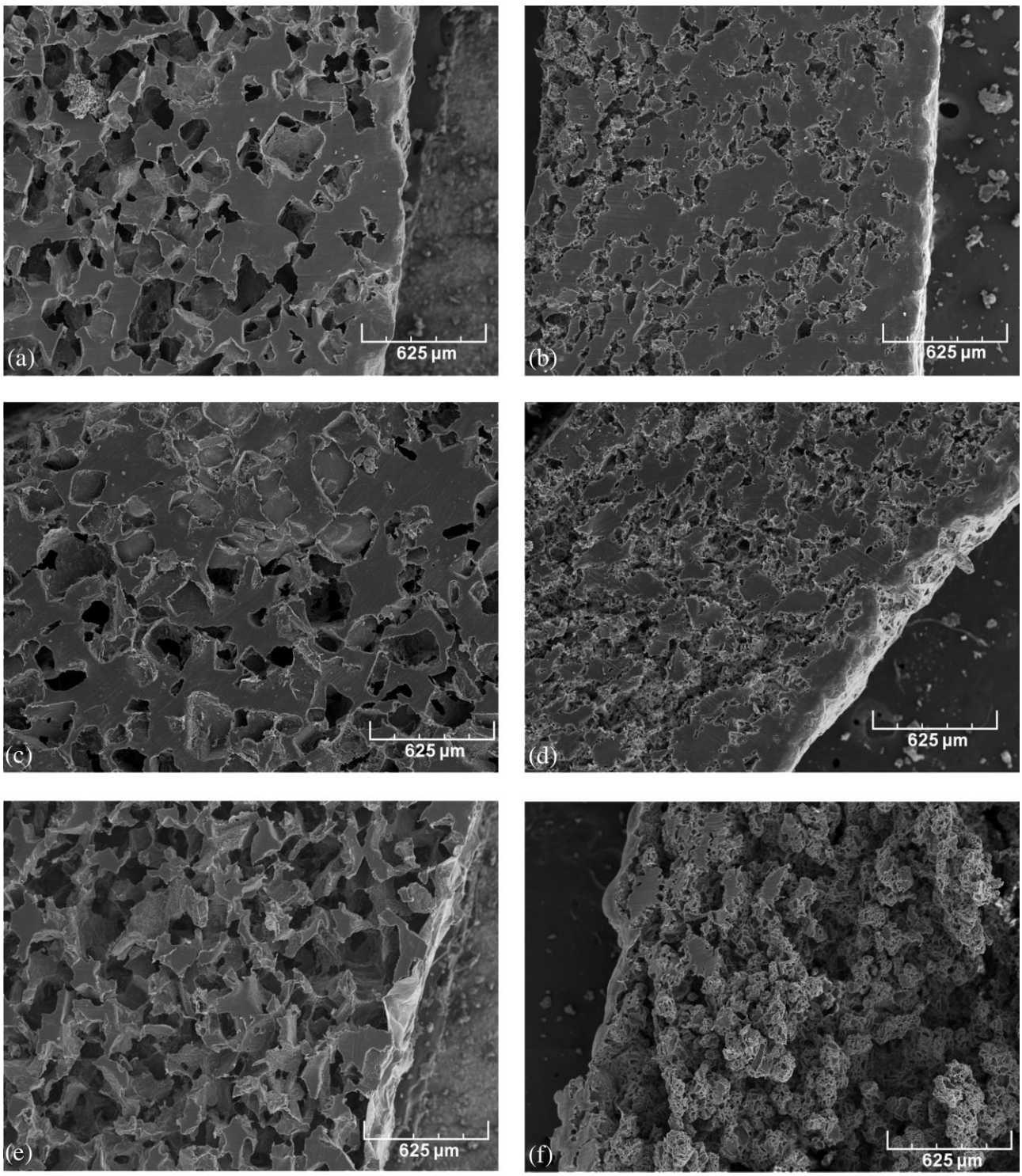

Figure 3 SEM images of porous UHMWPE structures created through salt leaching. (a) Large pores, 30 vol %; (b) small pores, 30 vol %; (c) large pores, 50 vol %; (d) small pores, 50 vol %; (e) large pores, 63 vol %; (f) small pores, 70 vol %.

the polymer scaffolding while hiding the complex surface topography.

A variety of impregnated samples can be seen in Figure 5. In all samples, the gelatin was able to penetrate completely to the centermost regions of the circular cross-section. Samples made from smaller particles had regions of small-branched pores resulting in gelatin branches, which were thinly spread and not as bright in backscatter mode, making image analysis challenging. The samples made with large pores in the UHMWPE appeared to have a greater extent of volume filled with the gelatin phase.

Every sample also contained a fraction of unfilled voids. Figure 6 shows magnified images of voids

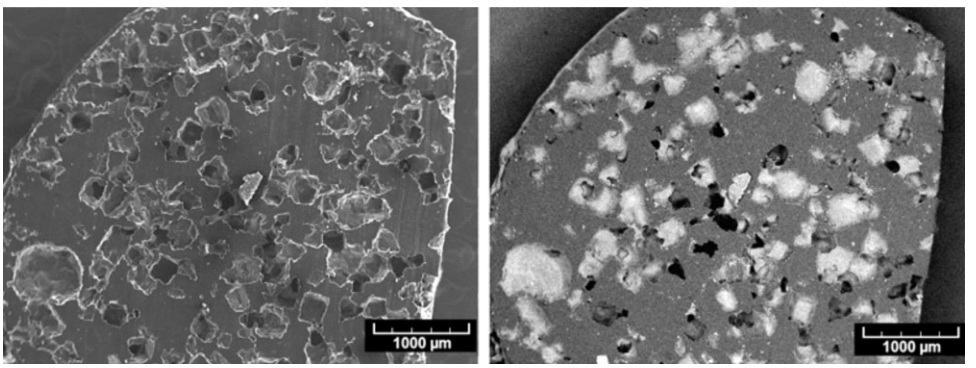

Figure 4 Secondary image (left) and backscattered image (right) of a 30% porous sample made from large NaCl particles. Pores successfully impregnated with gelatin glow brightly in backscattered images.

found in samples created with large pores. These images suggest two possible scenarios for void formation: (1) entrapped air bubbles or (2) channels which are too small for viscous gelatin to flow through. The first situation, entrapped air bubbles, is represented by the locations marked "a" in the figure and is characterized by a void that is surrounded by gelatin along part of its boundary. This interface creates a markedly smooth and rounded surface on the gelatin, making their occurrence easy to identify. It is hypothesized that better saturation of the porous scaffold might be achieved by degassing the gelatin before impregnation, keeping the gelatin warm to decrease viscosity during the impregnation process, or applying the vacuum for longer during the curing process. Mechanical agitation during the impregnation process might also be beneficial by coercing air bubbles to find paths to the external surface of the scaffold. These entrapped air bubbles account for the majority of voids visible in all samples.

The voids at locations identified as "b" appear to be completely isolated from all other pores, or only connected to another pore through a very small channel. These types are much more difficult to identify because of the limited view of the SEM into the three-dimensional porous structure. It is possible that these voids are simply extensions of trapped air pockets, and the identifiable interfaces are either hidden beneath the surface or were removed during

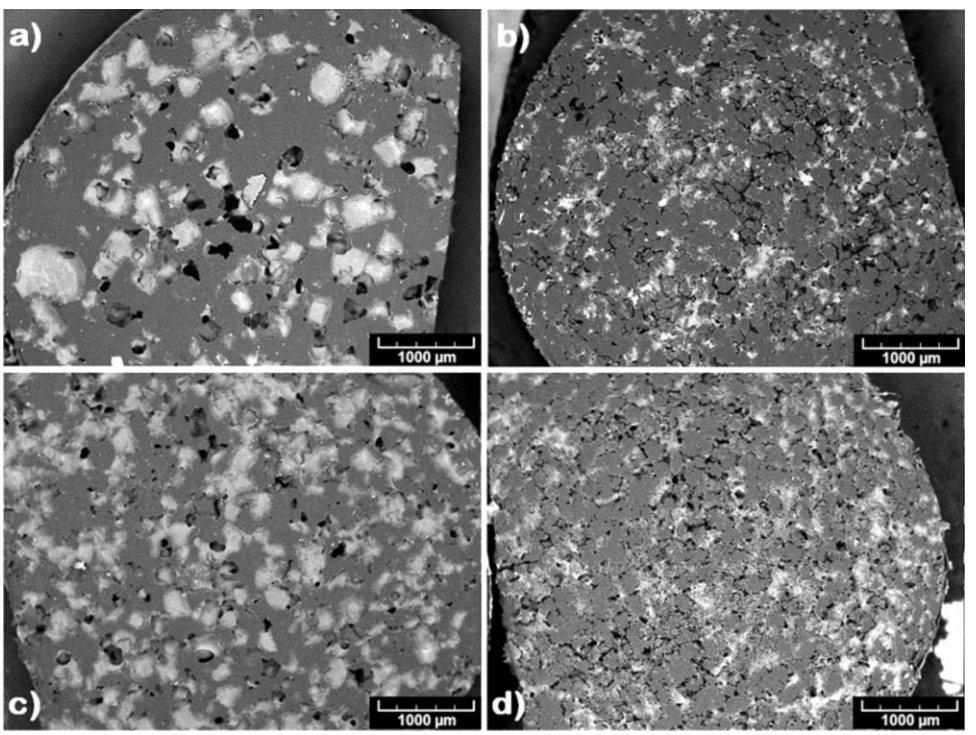

Figure 5 Comparison of gelatin penetration for samples made with (a) 30% porous, large particles; (b) 30% porous, small particles; (c) 50% porous, large particles; (d) 50% porous, small particles.

sample preparation. A second possibility is that neighboring pores were only interconnected by small channels through which water could flow during the leaching process, but the more viscous gelatin was unable to flow through. Figure 7 demonstrates the limitations of gelatin flow through small channels. The channel at location "c" measures $\sim$ 20 μm in width and is clearly large enough for gelatin to flow through. The neighboring channel at "d" measures $\sim$ 10 μm in width, small enough to prevent gelatin flow. A few of the same basic strategies suggested to eliminate air bubble entrapment may benefit small channel flow as well, most notable increasing the impregnation temperature of the gelatin phase to reduce its viscosity. It is important to note, however, that with protein-based materials elevated temperature may denature the microstructure and thus significantly alter the physical properties of the gels. This tradeoff between impregnation quality and protein damage must be investigated.

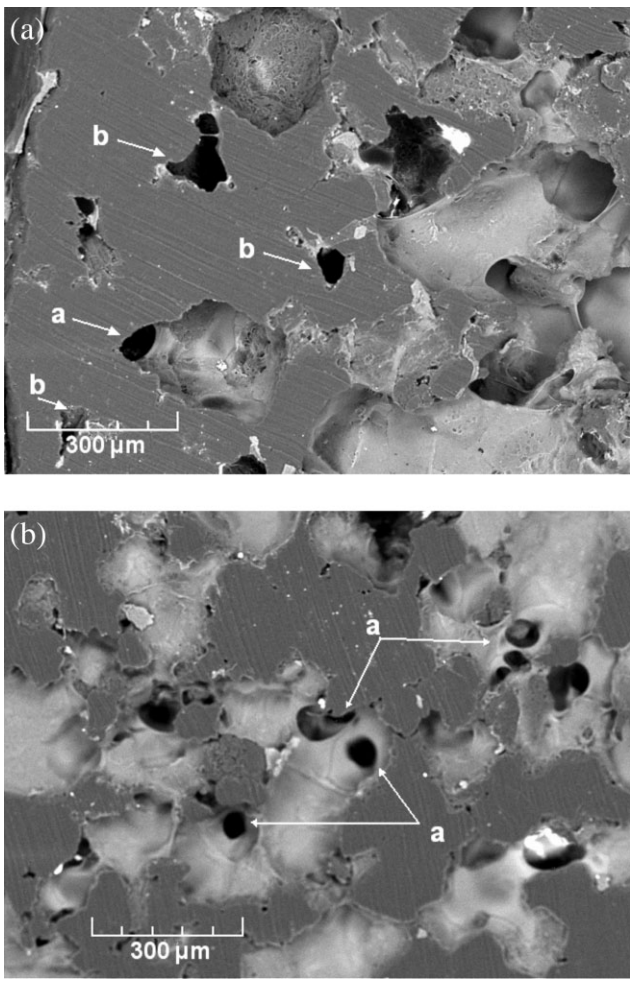

Figure 6 Backscattered images of voids in a porous sample made using large NaCl particles. The void at location (a) represents a pocket of air entrapped by gelatin, whereas the void at (b) shows no presence of gelatin within the pore.

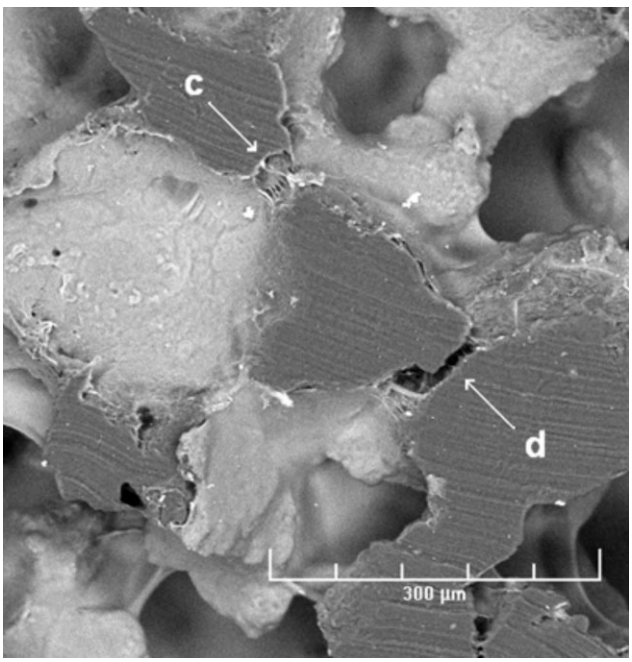

Figure 7 Gelatin can flow through the narrow channel at (c), which measures 20 μm across. However, gelatin does not flow through channel (d), which measures only 10 μm across.

Regardless of the quantity and cause of voids within the composite, it is apparent that for every case in this study, the gelatin phase was able to permeate throughout the majority of the UHMWPE scaffold, and the gelatin conformed to the size and geometry of the pores within the scaffold. This opens the door for future research using porous UHMWPE as scaffolding for other hydrogels and bioderived polymers.

CONCLUSIONS

1. Controlled, porous UHMWPE morphologies can be produced by dry mixing of NaCl porogen and polymer powder followed by compression molding.
2. Porogen particles will be well dispersed when they are similar in size to the UHMWPE particles. However, vein-like porogen accumulations seen in the samples of mismatched particle sizes allow for more complete removal of NaCl through the leaching process.
3. Porous UHMWPE morphologies can be impregnated with a gel-phase that initially has sufficiently low viscosity to allow for penetration of the void network in the polymer.
4. The use of colloidal gold and subsequent critical-point drying are well suited for SEM imaging and determination of gel-phase permeation into porous UHMWPE composites.

References

1. Dumbleton, J. H.; Manley, M. T.; Edidin, A. A. J Arthroplasty 2002, 17, 649.
2. Chiesa, R.; Tanzi, M. C. J Biomed Mater Res 2000, 50, 381.
3. Muratoglu, O. K.; O'Connor, D. O.; Bragdon, C. R.; Delaney, J.; Jasty, M.; Harris, W. H.; Merrill, E.; Venugopalan, P. Biomaterials 2002, 23, 717.
4. Jasty, M.; Rubash, H. E.; Muratoglu, O. J Arthroplasty 2005, 20, 55.
5. Oral, E.; Christensen, S. D.; Malhi, A. S.; Wannomae, K. K.; Muratoglu, O. K. J Arthroplasty 2006, 21, 580.
6. Ries, M. D. J Arthroplasty 2005, 20, 59.
7. Chiesa, R.; Moscatelli, M.; Gonzalez-Mora, V.; Hoffman, M.; Stroosnijder, M. F.; Tanzi, M. C.; Cigada, A. Molecular, cellular and Tissue Engineering. In Proceedings of the IEEE-EMBS special Topic Conference, 2002, p 58.
8. Lewis, G. Biomaterials 2001, 22, 371.
9. Pruitt, L. A.; Pruitt, L. A. Biomaterials 2005, 26, 905.
10. Tanniru, M.; Misra, R. D. K. Mater Sci Eng A 2005, 405, 178.
11. Guofang, G.; Guofang, G.; Huayong, Y.; Xin, F. Wear 2004, 256, 88.
12. Xie, X. L.; Tang, C. Y.; Chan, K. Biomaterials 2003, 24, 1889.
13. Xiong, D. S.; Lin, J. M.; Fan, D. L. Biomed Mater 2006, 1, 175.
14. Schwartz, C. J.; Bahadur, S.; Mallapragada, S. K. Wear 2007, 263, 1072.
15. Dangsheng, X.; Dangsheng, X. Mater Lett 2005, 59, 175.
16. Xue, Y.; Wu, W.; Jacobs, O.; Schadel, B. Polym Test 2006, 25, 221.
17. Schwartz, C.; Bahadur, S. Wear 2007, 262, 331.
18. Liu, G. D.; Xiang, M.; Li, H. L. Polym Eng Sci 2004, 44, 197.
19. Khorasani, M. T.; Zaghiyan, M.; Mirzadeh, H. Colloids Surf B: Biointerfaces 2005, 41, 169.
20. Zhang, M.; Pare, P.; King, R. J Biomed Mater Res 2007, 82, 18.
21. Fang, L.; Fang, L.; Gao, P.; Leng, Y. Compos B 2007, 38, 345.
22. Matthews, J. B.; Besong, A. A.; Green, T. R.; Stone, M. H.; Wroblewski, M.; Fisher, J.; Ingham, E. J Biomed Mater Res 2000, 52, 296.
23. Green, T. R.; Fisher, J.; Matthews, J. B.; Stone, M. H.; Ingham, E. J Biomed Mater Res 2000, 53, 490.
24. Tipper, J. L.; Galvin, A. L.; Williams, S. J Biomed Mater Res 2006, 78, 473.
25. Zhu, Y. H.; Chiu, K. Y.; Tang, W. M. J Orthop Surg (Hong Kong) 2001, 9, 91.
26. Drury, J. L.; Mooney, D. J. Biomaterials 2003, 24, 4337.
27. Oka, M.; Ushio, K.; Kumar, P.; Ikeuchi, K.; Hyon, S.; Nakamura, T.; Fujita, H. Proc Inst Mech Eng Part H: J Eng Med 2000, 214, 59.
28. Suciu, A. N.; Iwatsubo, T.; Matsuda, M.; Nishino, T. JSME Int J Ser C 2004, 47, 199.
29. Freeman, M. E.; Furey, M. J.; Love, B. J.; Hampton, J. M. Wear 2000, 241, 129.
30. Dawlee, S.; Sugandhi, A.; Balakrishnan, B.; Labarre, D.; Jayakrishnan, A. Biomacromolecules 2005, 6, 2040.
31. Leach, J. B.; Bivens, K. A.; Patrick, C. W., Jr.; Schmidt, C. E. Biotechnol Bioeng 2003, 82, 578.
32. Li, Q.; Williams, C. G.; Sun, D. D. N.; Wang, J.; Leong, K.; Elisseeff, J. H. J Biomed Mater Res A 2004, 68, 28.
33. Wellisz, T. Aesthetic Plast Surg 1993, 17, 339.
34. Elyashevich, G. K.; Olifirenko, A. S.; Pimenov, A. V. Desalination 2005, 184, 273.
35. Hou, Q.; Grijpma, D. W.; Feijen, J. Biomaterials 2003, 24, 1937.
36. Katoh, K.; Tanabe, T.; Yamauchi, K. Biomaterials 2004, 25, 4255.
37. Liao, C.-J.; Chen, C.-F.; Chen, J.-H. J Biomed Mater Res 2002, 59, 676.
38. Shutov, F.; Ananthanarayan, V. T. J Cell Plast 2002, 38, 163.
39. Draghi, L.; Resta, S.; Pirozzolo, M. G.; Tanzi, M. C. J Mater Sci Mater Med 2005, 16, 1093.
40. Reignier, J.; Huneault, M. A. Polymer 2006, 47, 4703.
41. Brown, G. M.; Butler, J. H. Polymer 1997, 38, 3937.